Chalcogenide Letters Vol. 13, No. 2, February 2016, p. 79 - 89

PHASE SEPARATION AND CRYSTALLIZATION KINETICS STUDIES OF AMORPHOUS $Si_{10}Te_{90}$

A. A. JORAID[a,*] , M. ABU EL-OYOUN[b], N. AFIFY[b]
[a]*Department of Physics, Taibah University, Madinah, Saudi Arabia*
[b]*Department of Physics, Assiut University, Assiut, Egypt*

The kinetic parameters of two overlapping crystallization peaks of $Si_{10}Te_{90}$ chalcogenide glass were studied using differential scanning calorimetry (DSC). The present study was conducted under experimental non-isothermal and predicted isothermal conditions. The experimental data were analysed using the Friedman differential isoconversional method. The dependence of the effective activation energy of crystallization on the extent of the crystallization indicates a clear difference between the two peaks. The Avrami–Erofeev reaction model reaction may describe the crystallization process of the two peaks of the chalcogenide glass under investigation. The reaction model of the first peak was found to be independent of temperature and was nearly equal to A6. However, the reaction model for the second peak varies from A2 to A6 as the temperature increases from 300 to 350 K.

(Received December 21, 2015; Accepted February 29, 2016)

Keywords: DSC; Crystallization kinetics; Kinetic parameters; Nonisothermal; Prediction isothermal; Reaction model

1. Introduction

The growing interest in chalcogenide glasses has been partially stimulated by their interesting electrical and optical properties and hence their wide scientific and technological applications. These properties are typically connected via crystallization. In chalcogenide glassy systems, glasses undergoing exothermic crystallization above the glass transition temperature appear to be of the memory switching type. Memory switching arises from the boundaries of glass-forming regions where glasses are more likely to crystallize [1-7]. Many glasses based on silicon-tellurium (Si-Te) system exhibit switching phenomena. Hence, crystallization of the Si-Te binary system has been intensely investigated [8-14].

Continuing our previous work [15,16], we study the crystallization kinetics of a system that exhibits a single, well-defined broad peak and was formed by the overlapping of two exothermic crystallization curves. In this work, the kinetic parameters (i.e., the activation energy E, the pre-exponential factor A and the Avrami exponent n) of the two overlapping $Si_{10}Te_{90}$ crystallization peaks were studied using differential scanning calorimetry (DSC), under non-isothermal conditions for a wide range of heating rates (5–90 K min^{-1}). The kinetic parameters were calculated from the DSC data using AKTS-Thermokinetics software [17] and isoconversional (model-free) analyses.

2. Experiment

Melt-quench technique was used to prepare the bulk material of $Si_{10}Te_{90}$ chalcogenide glass. High-purity (99.999%) Si and Te in proper at.% quantities were weighed and sealed in a quartz-glass ampoule (12 mm diameter) under a vacuum of 0.01 Pa. The ampoule was heated up to 1,220 K for 24 h in a rocking furnace then quenched in ice water.

*Corresponding author: aaljoraid@taibahu.edu.sa

The DSC experiments were carried out using a Shimadzu DSC-50 differential scanning calorimeter with an accuracy of ± 10 W. A small bulk samples (5 mg) were sealed in aluminum pans and scanned under dry nitrogen atmosphere at a rate of $50\ \mathrm{ml\ min^{-1}}$ and selected heating rates β of 5, 10, 15, 20, 25, 30, 40, 50, 60, 70, 80, and 90 $\mathrm{K\ min^{-1}}$. Indium $\left(T_{\mathrm{m}} = 429.6\ \mathrm{K}, \Delta H_{\mathrm{m}} = 28.55\ \mathrm{Jg^{-1}}\right)$ at a heating rate of 10 K min^{-1} was used to calibrate the temperature and enthalpy. Specific heat treatment was not used to nucleate the samples prior to the thermal analysis run.

The kinetics analysis in this study was conducted using the advanced thermokinetics software from Advanced Kinetics and Technology Solutions, Switzerland (AKTS-Thermokinetics ver. 4.02) [17]. Calculations with AKTS software increases the accuracy of the estimated kinetic parameters because it is simultaneously optimizes the baseline of data curves. The software applies isoconversional method for kinetic analysis.

3. Theoretical background

The crystallization reaction rate equation is usually based on the temperature T and conversion fraction (reaction progress) α. The kinetic equation combined with the Arrhenius expression is [18-20]:

$$\frac{\mathrm{d}\alpha}{\mathrm{d}t} = k\left(T\right) f\left(\alpha\right) = A\exp\left(-\frac{E}{RT\left(t\right)}\right) f\left(\alpha\right), \tag{1}$$

where k is the reaction rate constant, t(s) is the time, $f(\alpha)$ is the reaction model, A(s^{-1}) is the pre-exponential (frequency) factor, E (kJ mol^{-1}) is the effective activation energy and R is the universal gas constant. The three parameters associated with the energy barrier, the frequency of vibrations of the activated complex, and the reaction mechanism are the pre-exponential factor A, the effective activation energy E, and the reaction model $f(\alpha)$, respectively. Together, these are referred to as the "kinetic triplet". The crystallization process is generally well understood when the kinetic triplet is known.

The isoconversion method can be used to obtain accurate and consistent kinetic information for both nonisothermal and isothermal processes. This method implies that the reaction rate at a constant conversion, α, is a function of temperature only. By taking the logarithmic derivative of the reaction rate given by Eq. 1 at α = constant, we obtain:

$$\left[\frac{\partial\ln\left(\mathrm{d}\alpha/\mathrm{d}t\right)}{\partial\left(T^{-1}\right)}\right]_{\alpha} = \left[\frac{\partial\ln\left(k\left(T\right)\right)}{\partial\left(T^{-1}\right)}\right]_{\alpha} + \left[\frac{\partial\ln\left(f\left(\alpha\right)\right)}{\partial\left(T^{-1}\right)}\right]_{\alpha}, \tag{2}$$

The conversion fraction α and the reaction model $f(\alpha)$ are constant, and thus, the second term on the right-hand side of Eq. 2 is zero. Thus,

$$\left[\frac{\partial\ln\left(\mathrm{d}\alpha/\mathrm{d}t\right)}{\partial\left(T^{-1}\right)}\right]_{\alpha} = -\frac{E\left(\alpha\right)}{R}. \tag{3}$$

Hence, the use of isoconversional "model-free" method to extract the effective activation energy $E(\alpha)$ does not require any sort of the reaction model $f(\alpha)$.

The differential isoconversional approach of Friedman [21] can be obtained by taking the logarithm of the conversion rate dα/dt as a function of the reciprocal temperature at any conversion

α. For various heating rates β_i and at a specific degree of conversion α, the Friedman method is given by [19-21]

$$\ln\left(\frac{d\alpha}{dt}\right)_{\alpha i} = \ln\left(A_\alpha\, f\,(\alpha)\right) - \frac{E_\alpha}{RT_{\alpha i}}. \quad (4)$$

Therefore, plotting of $\ln(d\alpha/dt)$ against $1/T$ is a straight line with a slope $m = -E/R$ and an intercept equal to $\ln\left(A_\alpha\, f\,(\alpha)\right)$.

4. Results

The experimental measurements were conducted at heating 5, 10, 15, 20, 25, 30, 40.50, 60.70, 80 and 90 90 K min^{-1}. Results indicated the presence of one exothermic broad peak between 540 and 650 K for all heating rates. Fig. 1 shows the DSC curves obtained. When the DSC thermographs show a single well-defined broad crystallization peak, the probability of overlapping between two or more curves cannot be ignored. At heating rates of < 20 K min^{-1}, the crystallization curve consists of two peaks. As the heating rate increases to > 30 K min^{-1}, these two peaks merge into one peak. Figs. 2a, 2b and 2c show examples of the separation of overlapped crystallization exothermal curves recorded at constant heating rates of 5, 25 and 90 K min^{-1}, respectively. Henceforth, the first and second peaks are designated as P1 and P2, respectively.

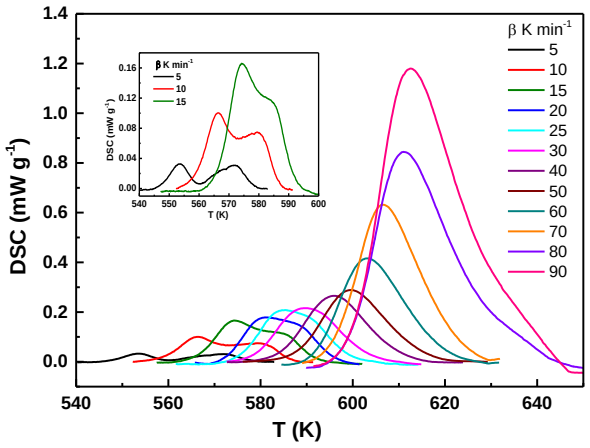

Fig. 1. Typical DSC trace of amorphous $Si_{10}Te_{90}$ glasses at β = 5-90 K min^{-1}.

5. Discussion

The results of the derived percentage contribution of the separated peaks to the total curve area shown in Fig. 2 were found to be highly similar for all heating rates and equal to 44% and 56% for P1 and P2, respectively. The observed non-symmetric DSC crystallization peaks of $Si_{10}Te_{90}$ suggest multiphase crystallization.

Deconvolution of the DSC crystallization peak showed two individual peaks with distinct maxima temperature, T_{P1} and T_{P2} for P1 and P2, respectively.

Under these situations, the DSC crystallization peak was treated as a convolution of two individual peaks with distinct maxima temperature, T_{P1} and T_{P2} for P1 and P2, respectively. The occurrence of double glass transition and double-stage crystallization in Si_xTe_{100-x} glasses with $10 \le x \le 20$ was demonstrated previously [8]. The phenomenon of double-stage crystallization was found to occur in a variety of chalcogenide glasses, such as Ge-As-Se-Te [22], Ge-Te-Sb [23],

Ga-Sb-S [24], Se-Te-Ag [25], Se-Ge-Pb [26], Se-Te-Sn [27] and Se-Te-Sb [28]. The phenomenon of double crystallization peaks is a direct result of the phase separation occurring in glasses [8]. An example of the results of the deconvolution are displayed in Fig. 2 (a, b and c), with the solid line representing the Gaussian function of (P1) and (P2). The peak of the first change (P1) was observed between 553 and 611 K for a heating rate of 5–90 K min^{-1}, and the peak of the second change (P2) was observed between 570.5 and 619 K for the same heating rate range.

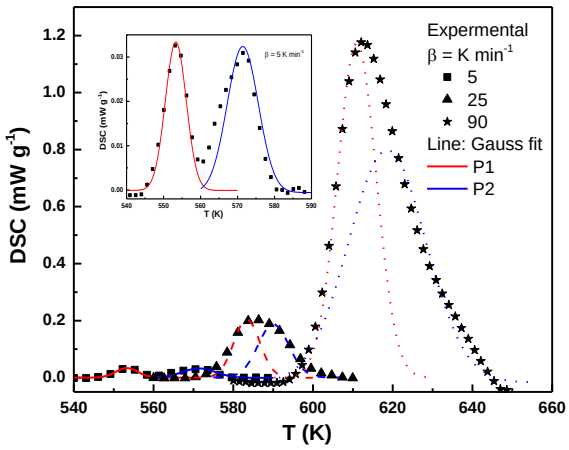

Fig. 2. Example of the separation of overlapped crystallization exothermal curves recorded at a constant heating rate of 5, 25 and 90 K min^{-1}

5.1 Effective activation energy for crystallization

This section discusses the kinetic analysis of crystallization events for the two peaks. To calculate the effective activation energy *E* for the crystallization, the Friedman equation (Eq. (4)) was used over a conversion range of $\alpha = 0.5$ at different heating rates β_i. The plots of $\ln(d\alpha/dt)_{\alpha i}$ against $10^3/T_{\alpha i}$ are shown in Fig. 3 for both peaks (P1 and P2). The data can be fitted into a straight line for both peaks (P1 and P2), leading to two different values of the effective activation energy for crystallization, 123.9 and 144.7 kJ mol^{-1} for P1 and P2, respectively. The dependences of the experimental value of the effective activation energy of crystallization E_α and of the experimental value of $\ln(A_\alpha f(\alpha))$ on the extent of crystallization α, obtained using Eq. 4 for the two peaks (P1 and P2), are shown in Fig. 4.

The plot of activation energy for crystallization E_α revealed a clear difference between the two peaks (P1 and P2) with respect to the reaction progress α. For (P1), the activation energy E_α is mostly independent of the value of α, only exhibiting somewhat sudden small changes in the terminal stage of the crystallization. However, the second peak (P2) is characterized by a sharp decrease in E_α with the reaction progress α; this decrease continued toward the end of the reaction and was followed by a small increase at $\alpha > 0.8$. The behaviour of $E(\alpha)$ for P1 and P2 is in good agreement with the results of our previous study, where the first and second peaks were clearly separated [15].

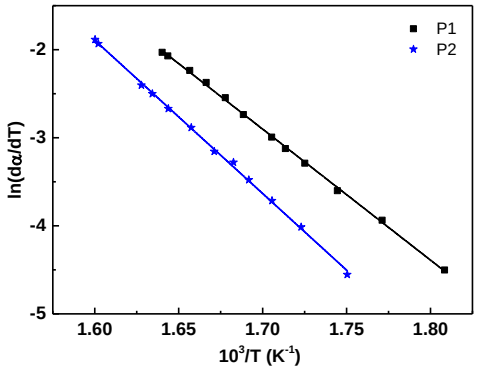

Fig. 3. Plots of $\ln\left(\mathrm{d}\alpha/\mathrm{d}t\right)_{\alpha\mathrm{i}}$ *against* $10^3/T_{\alpha\mathrm{i}}$ *for the P1 and P2 peaks*

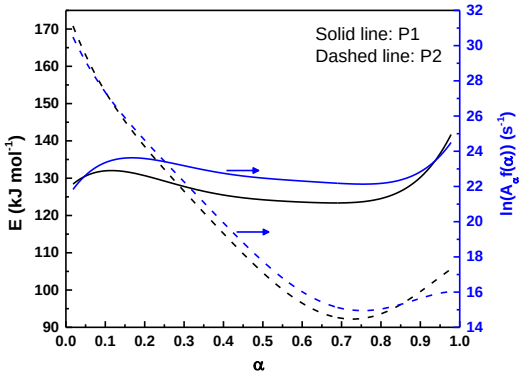

Fig. 4. Dependence of the activation energy of crystallization E_α *and of the experimental* $\ln\left(A_\alpha\ f\ (\alpha)\right)$ *values on the extent of crystallization* α

The pre-exponential factor $A(\mathrm{s}^{-1})$ was expressed as $\ln\left(A_\alpha\ f\ (\alpha)\right)$ for the two peaks. The dependence of the activation energy for crystallization E_α, on the temperatures for the two peaks (P1 and P2) is shown in Fig. 5. The values of E_α remain fairly constant throughout the entire temperature interval for P1. In contrast, the E_α values for P2 show a strong temperature dependence.

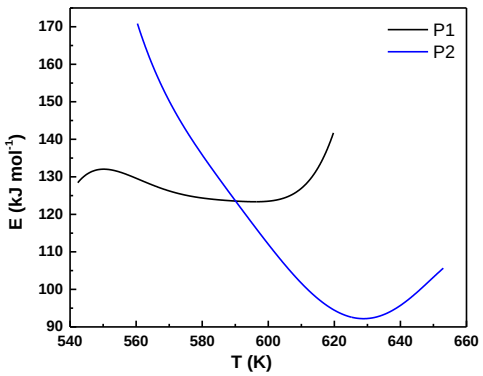

Fig. 5. Dependence of the activation energy of crystallization E_α *on the temperature.*

The value of E_α decreases from approximately 170 kJ mol^{-1} at T=561 K to 92 kJ mol^{-1} at 629 K. Such high variations in the activation energy with temperature gave evidence that the rate constant of the crystallization is determined by the rates of two processes: nucleation and diffusion [15,29]. However, due to the dependence of E_α on temperature, for P1, the value of E_α at $\alpha = 0.5$ is approximately 124.3 kJ mol^{-1}, which is close to the value of 123.9 kJ mol^{-1} obtained using the Friedman plot shown in Fig. 3. Additionally, for P2, the value of E_α at $\alpha = 0.5$ is approximately 104.6 kJ mol^{-1}, which is lower than the value of 144.7 kJ mol^{-1} obtained using the Friedman plot discussed above.

5.2 Prediction of the reaction progress under isothermal conditions

Because the activation energy and pre-exponential factor of the examined materials were determined from nonisothermal experiments, the extent of the reaction progress α could be determined under any temperature mode, including the isothermal mode [30-35]. The predictions for the isothermal conversion fraction α of P1 and P2 for the samples under investigation are shown in Fig. 6.

However, a combination of nonisothermal and isothermal experiments is one of the most accurate techniques to determine the kinetic parameters [19]. The isothermal crystallization kinetics of $Si_{10}Te_{90}$ glasses were analysed based on the well-known Avrami equation [36-38]. The double logarithmic form of this equation is given as:

$$\ln\left[-\ln\left(1-\alpha_t\right)\right] = n\ln k + n\ln t\,, \tag{5}$$

where n is the Avrami exponent and k is the overall kinetic rate constant. Both k and n depend on the nucleation mechanism and growth geometry. The values of n and k are determined from Eq. (7) by least squares fitting of $\ln\left[-\ln\left(1-\alpha_t\right)\right]$ versus $\ln t$. The double natural logarithmic plots for the Avrami analysis are shown for the first and second peaks at different crystallization temperatures in Fig. 7. The obtained values of the Avrami exponent n and overall kinetic rate constant k are shown in Fig. 8.

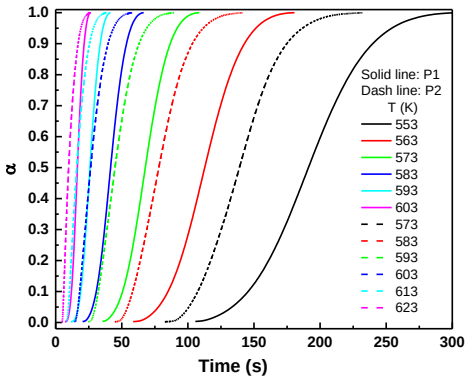

Fig. 6. Predicted isothermal crystallization fractions α over time for different temperatures

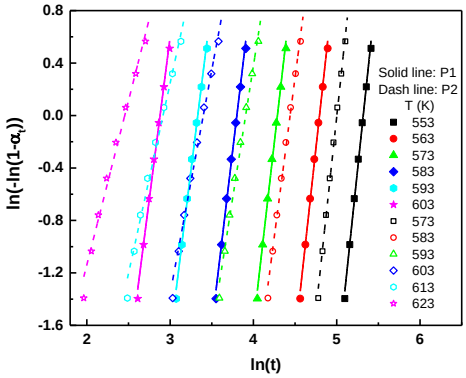

Fig. 7. Plots of $\ln\left[-\ln\left(1-\alpha_t\right)\right]$ *versus* $\ln t$ *for the predicted isothermal crystallization fractions,* α*, at different temperatures*

The Avrami exponents indicate that the mechanism of crystallization for P1 is mainly that of multi-dimensional growth, with an average *n* value of 5.5. The unexpectedly high value of the Avrami exponent (*n* = 5.5) arises because both the nucleation frequency and crystal growth rate exhibit a power law dependence on time [15,39,40].
Generally, *n* should not exceed 4; nevertheless, high values of *n* have been reported for some systems [34]. The value of *n* for P2 shows a strong temperature dependence, with an average *n* value of 3.8.

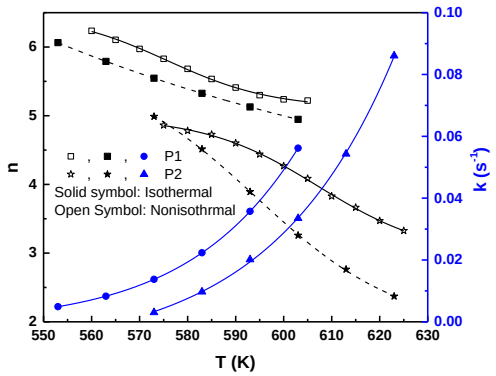

Fig. 8. Dependence of the Avrami exponent n on the temperature obtained from isothermal and nonisothermal conditions. The figure also shows the overall kinetic rate constant k against temperature.

It is recommended to compare the isothermal prediction results with those calculated using the nonisothermal equation suggested by Matusita et al. [41]. The Avrami exponent *n* can be obtained using this equation as [35]:

$$n = -\left.\frac{\mathrm{d}\left\{\ln\left[-\ln\left(1-\alpha\right)\right]\right\}}{\mathrm{d}\left(\ln\beta\right)}\right|_T, \tag{6}$$

As is evident from Fig. 8, the predicted and actual experimental results are nearly identical. The nonisothermal values of the Avrami exponent *n* are somewhat higher than the isothermal values. The average values of *n* for P1 were found to be 5.5 ± 0.3 and 5.7 ± 0.3 for

the isothermal and nonisothermal methods, respectively, whereas for P2, the average values were found to be 3.6 ± 0.2 and 4.5 ± 0.3 for the isothermal and nonisothermal methods, respectively. The details of the crystallization process was investigated by using the local Avrami exponent $n(\alpha)$, which is given by [15,35]:

$$n(\alpha) = \frac{\partial \ln\left[-\ln(1-\alpha_t)\right]}{\partial \ln t}. \tag{7}$$

The value of $n(\alpha)$ offers information associated to the nucleation and growth behaviour for the reaction progress α. The values of $n(\alpha)$ at different temperatures for P1 and P2 as a function of the conversion fraction α are shown in Fig. 9.

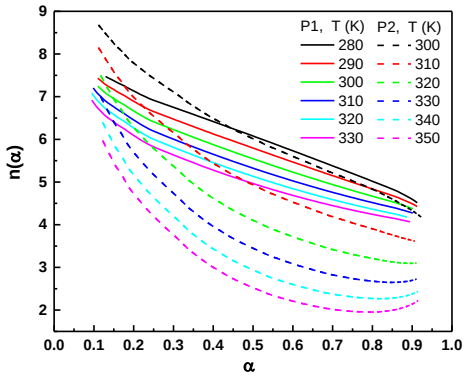

Fig. 9. Local Avrami exponent n(α) versus the crystallized fraction α at different temperatures.

Table 1. Solid-state reaction models of Avrami-Erofeev used to describe the crystallization process.

Model Notation	$g(\alpha)$	Avrami exponent, *n*
A1.5	$\left[-\ln(1-\alpha)\right]^{2/3}$	1.5
A2	$\left[-\ln(1-\alpha)\right]^{1/2}$	2
A3	$\left[-\ln(1-\alpha)\right]^{1/3}$	3
A4	$\left[-\ln(1-\alpha)\right]^{1/4}$	4

The $n(\alpha)$ values clearly decreased with an increasing conversion fraction α for each temperature range and decreased with increasing temperature. The average local Avrami exponent $n(\alpha)$ values were found to be 5.7 and 4.3 for P1 and P2, respectively, in good agreement with the values discussed above. However, comparing Figures 8 and 9, the Avrami exponent *n* shows a dramatic difference between P1 and P2. For P1, *n* decreases slightly with increasing temperature or reaction progress, and its value remains high at approximately 5.5. This indicates that the crystallization of P1 is mostly governed by three-dimensional growth. In contrast, for P2, the Avrami exponent strongly decreases with increasing temperature or reaction progress, and its value varies between approximately 5 and 2.

To verify the existence of the deduced dimensional growth, the crystallization process is described by using the reduced reaction model $g(\alpha)$ (Table 1). The conversion fraction (reaction

progress) α depends on several factors, such as nucleation, diffusion and geometrical shape. These factors led to the development of many solid-state reaction models. In particular, the Avrami-Erofeyev model is shown in Table 1 [18-20,34,35]. The reduced reaction model $g(\alpha)$ for isothermal kinetics is given by [34,35,42,43]

$$g(\alpha) = B\,\frac{t}{t_{\alpha=0.632}}, \tag{8}$$

where B is a constant equal to one and dependent on the form of function $g(\alpha)$. The time required to reach a specific reaction progress t_{α} was calculated at $\alpha = 0.632$ because the reduced activation energy (E/RT) approaches infinity at this value [34,35].

We use the $g(\alpha)$ values obtained using experimental data and Eq. 8 and the values obtained by theoretical models obtained from Table 1 to generate Fig. 10; this figure shows the plot of $g(\alpha)$ versus the conversion fraction α. The reactions models for both peaks P1 and P2 undoubtedly follow the Avrami–Erofeev mechanism. On the other hand, for P1 and in the case of solid-state reaction models, the analysis clearly indicates that the mechanism is strictly constant and is A6 for the entire range of examined temperatures (280-330 K); with the exception of the end of crystallization $(\alpha > 0.8)$, the mechanism remains confined between $4 < A < 6$. Nevertheless, for P2, the behaviour of the Avrami–Erofeev mechanism is dramatically different, as is clearly shown in Fig. 10. At low temperatures (300 K), the mechanism is nearly A6. As the temperature increases, the mechanism tends toward lower values and is almost A2.

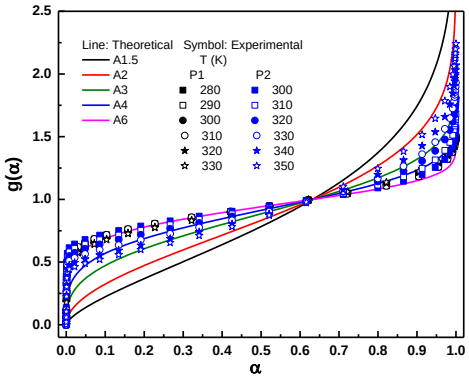

Fig. 10. Variation of the reduced reaction model $g(\alpha)$ with the degree of crystallization α for P1 and P2. The solid lines were calculated from the various theoretical models listed in Table 1.

Finally, Fig. 11 shows the sigmoidal shapes for the crystallization fraction for P1 and P2 of both the experimental and simulated results. Fig. 11 confirms the reliability of the obtained results because the experimental and simulated results are nearly identical.

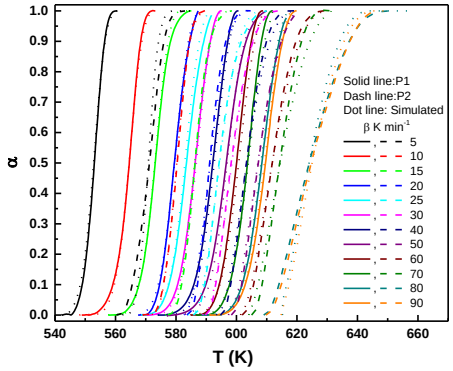

Fig. 11. Typical experimental and predicted results for the crystallization fraction sigmoidal shapes obtained at heating rate regime of β = 5-90 K min^{-1} for P1 and P2.

6. Conclusions

In this study, two overlapping chalcogenide glass $Si_{10}Te_{90}$ crystallization peaks were split. The kinetics' parameters were studied under experimental nonisothermal and predicted isothermal conditions. The differential isoconversional (model-free) method of Friedman was used to calculate the kinetic parameters. The average effective activation energy values obtained for the first and second peaks (P1 and P2) were 123.9 and 144.7 kJ mol^{-1}, respectively. The activation energy $E(\alpha)$ values show a nearly constant variation throughout the entire interval of transformations for P1, in contrast to the values for P2, which show a strong dependence on the conversion fraction and temperature.

The variations of the pre-exponential factor *A* and Avrami exponent *n* with the conversion fraction and temperature were investigated. The isothermal and nonisothermal methods were used to calculate the Avrami exponent *n*. The average *n* values for P1 were found to be 5.5 ± 0.3 and 5.7 ± 0.3, whereas for P2 these were found to be 3.6 ± 0.2 and 4.5 ± 0.3 for the isothermal and nonisothermal methods, respectively.

The Avrami–Erofeev solid-state reaction model may accurately describe the transformation process of $Si_{10}Te_{90}$ chalcogenide glass for both P1 and P2. However, for P1, the model was found to be independent of temperature and follows the A6 mechanism, whereas for P2, the reaction model varies from A6 to A2 with increasing temperature.

The obtained kinetic parameters were accurate, as shown by the good agreement between the actual and predicted sigmoidal curves for the crystallization fraction with increasing temperature.

References

[1] S. R. Ovshinsky, Phys. Rev. Lett. **21**, 1450 (1968) -1453.
[2] S. Asokan, G. Parthasarathy, E.S.R. Gopal, J. Mater. Sci. Lett. **4**, 502 (1985) -504.
[3] T. Takamori, R. Roy, G.J. McCarthy, Mat. Res. Bull. **5**, 529 (1970) -540.
[4] J. A. Savage, J. Mater. Sci. **7,** 64 (1972).
[5] S.R. Gunti, A. Ayiriveetil, A. Sundarrajan, J. Solid State Chem. **184**, 3345 (2011).
[6] C. Das, G.M. Rao, S. Asokan, J. Non-Cryst. Solids **357,** 165 (2011).
[7] M. Upadhyay, S. Murugavel, J. Non-Cryst. Solids **368,** 34 (2013).
[8] S. Asokan, G. Parthasarathy, E.S.R. Gopal, J. Non-Cryst. Solids **86,** 48 (1986).
[9] S. Asokan, G. Parthasarathy, G.N. Subbanna, E.S.R. Gopal, J. Phys. Chem. Solids **41,** 341 (1986).
[10] S. Asokan, E.S.R. Gopal, G. Parthasarathy, Key engineering Materials, **13-15,** 119 (1987).
[11] M.K. Gauer, I. Dezsi, U. Gonser, G. Langouche, H. Ruppersberg, Journal of Non-Crystalline

Solids **109**, 247 (1989).
[12] S.N. Zhang, T.J. Zhu, X.B. Zhao, Physica B **403,** 3459 (2008).
[13] R.D. Vengrenovitch, S.V. Podolyanchuk, I.A. Lopatniuk, M.O. Stasik, S.D. Tkachova, J. Non-Cryst. Solids **171,** 243 (1994).
[14] Yuta Saito, Yuji Sutou, Junichi Koike, Thin Solid Films **520,** 2128 (2012).
[15] M. Abu El-Oyoun, Mater. Chem. Phys. **131,** 495 (2011).
[16] A. H. Moharram M. Abu El-Oyoun, Appl. Phys. A **116**, 311 (2014).
[17] AKTS-Thermokinetics Version 4.02, Advanced Kinetics and Technology Solutions, http://www.akts.com (AKTS-Thermokinetics software) (2014).
[18] A. Khawam, D.R. Flanagan, J. Phys. Chem. B **110**, 17315 (2006).
[19] S. Vyazovkin, A.K. Burnham, J.M. Criado, L.A. Pérez-Maqueda, C. Popescu, N. Sbirrazzuoli, Thermochim. Acta **520**, 1 (2011).
[20] J. Farjas, P. Roura, J. Therm. Anal. Calorim. **105,** 757 (2011).
[21] H.L. Friedman, Application to a phenolic plastic. J. Polym. Sci. C **6,** 183 (1964).
[22] V.S. Shiryaev, J.L. Adam, X.H. Zhang, J. Phys. Chem. Solids **65,** 1737 (2004).
[23] N. Ziani, M. Belhadji, L. Heireche, Z. Bouchaour, M. Belbachir, Physica B **358**, 132 (2005).
[24] A.A. Othman, H.H. Amer, M.A. Osman, A.Dahshan, J. Non-Cryst. Solids **351,** 130 (2005).
[25] N. Mehta, A. Kumar, Mater. Chem. Phys. **96**, 73 (2006).
[26] Deepika, P.K. Jain, K.S. Rathore, N.S. Saxena, J. Non-Cryst. Solids **355,** 1274 (2009).
[27] F. Abdel-Wahab, Physica B **406,** 1053 (2011).
[28] M.A. Abdel-Rahim, M.M. Hafiz, A.Z. Mahmoud, Prog. Nat. Sci.: Mater. Int. **25,** 169 (2015).
[29] S. Vyazovkin, I. Dranca, Chem. Phys. **207,** 20 (2006).
[30] A.K. Burnham, L.N. Dinh, J. Therm. Anal. Cal. **89**, 479 (2007).
[31] B. Roduit, L. Xia, P. Folly, B. Berger, J. Mathieu, A. Sarbach, H. Andres, M. Ramin, B. Vogelsanger, D. Spitzer, H. Moulard, D. Dilhan, J. Therm. Anal. Cal. **93,** 143 (2008).
[32] B. Roduit, W. Dermaut, A. Lunghi, P. Folly, B. Berger, A. Sarbach, J. Therm. Anal. Cal. **93**, 163 (2008).
[33] H. Eloussifi, J. Farjas, P. Roura, M. Dammak, J. Therm. Anal. Cal. **108,** 597 (2012).
[34] A.A. Joraid, A.A. Abu-Sehly, M. Abu-El-Oyoun, A.H. Mohamed, Chalcogenide Letters **10**, 303 (2013).
[35] A.A. Joraid, I.M.A. Alhosuini, Thermochim. Acta **595,** 28 (2014).
[34] M. Avrami, J. Chem. Phys. **7**, 1103 (1939).
[35] M. Avrami, J. Chem. Phys. **8,** 212 (1940).
[36] M. Avrami, J. Chem. Phys. **9,** 177 (1941).
[37] J.L. Cardenas-Leal, J. Vazquez, D.Garcia-G. Barreda, P.L. Lopez-Alemany, P. Villares, R. Jimenez-Garay, J. Alloys Compd. **479,** 210 (2009).
[38] J. Vazquez, J.L. Cardenas-Leal, D. Garcia-G. Barreda, R. Gonzalez-Palma, P.L. Lopez-Alemany, P. Villares, Physica B **405,** 4462 (2010).
[39] K. Matusita, T. Komatsu, R. Yokota, J. Mater. Sci. **19**, 291 (1984).
[40] A.C. Lua, J. Su, Polym. Degrad. Stabil. **91,** 144 (2006).
[41] S. Majumdar, I.G. Sharma, A.C. Bidaye, A.K. Suri, Thermochim. Acta **473**, 45 (2008).